PERVUSHIN, V. YU, TOLCHEV, A. V., DENISOVA, T. A., GERMAN, V. A. & KLESHCHEV, D. G. (1989). *Russ. J. Inorg. Chem.* **34**, 615–617.
PROTAS, P. J., MARNIER, G., BOULANGER, B. & MENAERT, B. (1989). *Acta Cryst.* C**45**, 1123–1125.
REYNOLDS, M. L. & WISEMAN, T. J. (1967). *J. Inorg. Nucl. Chem.* **29**, 1381–1384.
SHELDRICK, G. M. (1976). *SHELX76*. Program for crystal structure determination. Univ. of Cambridge, England.
SPEER, J. A. & GIBBS, G. V. (1976). *Am. Mineral.* **61**, 238–247.
TORDJMAN, I., MASSE, R. & GUITEL, J. C. (1974). *Z. Kristallogr.* **139**, 103–115.
WANG, S. L., WANG, C. C. & LII, K. H. (1989). *J. Solid State Chem.* **82**, 298–302.

Acta Cryst. (1993). B**49**, 435–443

Kikuchi Patterns, Index System and Inflation Properties of an $Al_{70}Co_{15}Ni_{15}$ Decagonal Quasicrystal*

BY YANFA YAN, RENHUI WANG, JIANIAN GUI AND MINGXING DAI

Laboratory of Material Physics, Department of Physics, Wuhan University, 430072 *Wuhan, People's Republic of China, and Beijing Laboratory of Electron Microscopy, Academia Sinica, PO Box* 2724, 100080 *Beijing, People's Republic of China*

(*Received* 26 *November* 1991; *accepted* 28 *September* 1992)

Abstract

The general principle of the projection method and an index scheme for decagonal phases are described systematically. Kikuchi-line patterns over a large angular range from an $Al_{70}Co_{15}Ni_{15}$ decagonal quasicrystal with a periodicity of 4 Å along the tenfold axis were obtained by connecting a series of large-angle convergent-beam electron diffraction patterns. Computer-simulated electron diffraction patterns of major zone axes and Kikuchi-line patterns covering the whole orientation triangle show good agreement with the patterns recorded experimentally. After discussion of the inflation and deflation properties, appropriate quasilattice parameters of $a = 6.6$ Å (or 2.5 Å), $c = 4.0$ Å for an $Al_{70}Co_{15}Ni_{15}$ decagonal quasicrystal are chosen that are suitable for atomic decoration of the quasilattice of the decagonal phase.

1. Introduction

Decagonal quasicrystals having tenfold rotational symmetry and one-dimensional translational symmetry along the tenfold axis have been reported in rapidly solidified alloys of Al–Mn (Bendersky, 1985; Chattopadhyay, Lele, Ranganathan, Subbanna & Thangaraj, 1985), Al–Fe (Fung, Yang, Zhou, Zhao, Zhan & Shen, 1986), Al–Co (Dong, Li & Kuo, 1987; Suryanarayana & Menon, 1987), Al–Pd (Idziak, Heiney & Bancel, 1987) and Al–Ni (Li & Kuo, 1988). The period along the tenfold axis was about 12 Å for Al–Mn and 16 Å for Al–Co, Al–Fe and Al–Pd. In addition, a periodicity of 4 Å along the tenfold axis has been reported in Al–Ni (Li & Kuo, 1988) and in the stable decagonal phases of AlCoCu and AlCoNi (Tsai, Inoue & Masumoto, 1989). In the system AlCoCu, He, Wu & Kuo (1988) found decagonal quasicrystals with periodicities of 4, 8, 12 and 16 Å corresponding to two-, four-, six- and eight-layer stackings, respectively.

The cut-and-projection method (Elser, 1985; Katz & Duneau, 1986; Jaric, 1986) affords an adequate indexing of diffraction patterns for the icosahedral quasicrystalline phase. Based on this method, an indexing scheme was described for the decagonal phase (Ho, 1986) and used by Koopmans, Schurer, van der Woude & Bronsveld (1987) and Thangaraj, Subbanna, Ranganathan & Chattopadhyay (1987) in the interpretation of their data for the Al–Mn decagonal phase. These authors support the concept of the derivation of an indexing model that has a periodic axis c by a distortion of the icosahedral vertex basis, to a pentagonal-bipyramid (PB) edge-vector basis (Ho, 1986). Choy, FitzGerald & Kalloniatis (1988) provided a more straightforward index system, which uses a planar pentagonal basis set plus the periodic axis. These two index systems are equivalent. Mandal & Lele (1989, 1991) generated the direct and reciprocal space of a one-dimensionally periodic quasicrystal by simultaneous distortion of the six-dimensional hypercubic cell along one of its edges and also of the icosahedron (formed by projection of the six-dimensional basis

* Project support by the National Natural Science Foundation of China.

0108-7681/93/030435-09$06.00

vectors on to physical space) along one of its vertex vectors. In addition, these authors proposed a six-dimensional lattice for the decagonal phase.

We introduce here a general principle of the projection method from which all necessary matrices for projection can easily be deduced after the basis set in physical space has been selected. This general principle is suitable for the description of the decagonal, octagonal and other two-dimensional quasicrystals, and also the icosahedral and cubic quasicrystals after some minor changes. By application of this general principle of the projection method to the case of the decagonal quasicrystals, we obtain an index system that is suitable for all known decagonal phases having different periodicities (4, 8, 12 and 16 Å). The first index in our index scheme is related to the periodic tenfold axis $A10$ of the decagonal quasicrystals.

In the previous reports, investigation was limited to the Al–Mn decagonal phase with its periodicity of 12 Å along the tenfold axis. With the assumption that 4 Å is the shortest period along the tenfold axis and that Kikuchi-line patterns provide more information than do selected-area electron diffraction (SAED) patterns, we studied Kikuchi-line patterns and SAED patterns of an $Al_{70}Co_{15}Ni_{15}$ decagonal phase with a period of 4 Å by selecting an appropriate straightforward index system. The computations provide good agreement with experiment.

2. Index scheme and inflation properties

2.1. *General principle of the projection method*

A decagonal quasilattice may be described by the projection of a six-dimensional cubic-tetragonal lattice with basis vectors $\tilde{\mathbf{e}} = [\tilde{\mathbf{e}}_1\tilde{\mathbf{e}}_2\tilde{\mathbf{e}}_3\tilde{\mathbf{e}}_4\tilde{\mathbf{e}}_5\tilde{\mathbf{e}}_6]$ into three-dimensional ($3D$) physical space. These basis vectors possess the metric tensor

$$\boldsymbol{G} = \tilde{\mathbf{e}}^T\tilde{\mathbf{e}} = A^2\begin{bmatrix} k^2 & 0 & 0 & 0 & 0 & 0 \\ 0 & 1 & 0 & 0 & 0 & 0 \\ 0 & 0 & 1 & 0 & 0 & 0 \\ 0 & 0 & 0 & 1 & 0 & 0 \\ 0 & 0 & 0 & 0 & 1 & 0 \\ 0 & 0 & 0 & 0 & 0 & 1 \end{bmatrix}, \tag{1}$$

where the superscript ^{T} means the transpose of the matrix. Equation (1) shows that these basis vectors are orthogonal to each other and their moduli are kA for $\tilde{\mathbf{e}}_1$ and A for $\tilde{\mathbf{e}}_j$ ($j = 2, 3, 4, 5, 6$).

The inverse of the metric $\boldsymbol{G}$ is

$$\boldsymbol{G}^{-1} = (1/A^2)\begin{bmatrix} 1/k^2 & 0 & 0 & 0 & 0 & 0 \\ 0 & 1 & 0 & 0 & 0 & 0 \\ 0 & 0 & 1 & 0 & 0 & 0 \\ 0 & 0 & 0 & 1 & 0 & 0 \\ 0 & 0 & 0 & 0 & 1 & 0 \\ 0 & 0 & 0 & 0 & 0 & 1 \end{bmatrix}, \tag{2}$$

from which we can construct the reciprocal basis vectors $\tilde{\mathbf{e}}^* = [\tilde{\mathbf{e}}_1^*\tilde{\mathbf{e}}_2^*\tilde{\mathbf{e}}_3^*\tilde{\mathbf{e}}_4^*\tilde{\mathbf{e}}_5^*\tilde{\mathbf{e}}_6^*]$,

$$\tilde{\mathbf{e}}^{*T} = \boldsymbol{G}^{-1}\tilde{\mathbf{e}}^T. \tag{3}$$

Therefore, the reciprocal basis vectors $\tilde{\mathbf{e}}_i^*$ are also orthogonal, with moduli of $1/kA$ for $\tilde{\mathbf{e}}_1^*$ and $1/A$ for the other $\tilde{\mathbf{e}}_j^*$.

We now introduce an inverse metric tensor

$$\boldsymbol{G}^* = \tilde{\mathbf{e}}^{*T}\tilde{\mathbf{e}}^*. \tag{4}$$

Insertion of (3) into (4) gives

$$\boldsymbol{G}^* = (\boldsymbol{G}^{-1})^T = \boldsymbol{G}^{-1}. \tag{5}$$

Let the orthogonal and normalized basis sets in the parallel (physical) space be $\mathbf{E}_1$, $\mathbf{E}_2$, $\mathbf{E}_3$ and that in the orthogonal (complementary) space be $\mathbf{E}_4$, $\mathbf{E}_5$, $\mathbf{E}_6$. Suppose the relationship between $\tilde{\mathbf{e}}$ and $\boldsymbol{E} = [\mathbf{E}_1\,\mathbf{E}_2\,\mathbf{E}_3\,\mathbf{E}_4\,\mathbf{E}_5\,\mathbf{E}_6]^T$ is

$$\tilde{\mathbf{e}}^T = A\begin{bmatrix} k & 0 & 0 & 0 & 0 & 0 \\ 0 & & & & & \\ 0 & & & & & \\ 0 & & & \boldsymbol{S} & & \\ 0 & & & & & \\ 0 & & & & & \end{bmatrix}\boldsymbol{E}^T, \tag{6a}$$

then we have

$$\tilde{\mathbf{e}}^{*T} = (1/A)\begin{bmatrix} 1/k & 0 & 0 & 0 & 0 & 0 \\ 0 & & & & & \\ 0 & & & & & \\ 0 & & & \boldsymbol{S} & & \\ 0 & & & & & \\ 0 & & & & & \end{bmatrix}\boldsymbol{E}^T \tag{6b}$$

where $\boldsymbol{S} = [\boldsymbol{S}_l\boldsymbol{S}_r]$, $\boldsymbol{S}_l$ and $\boldsymbol{S}_r$ are 5×5, 5×2 and 5×3 matrices, respectively.

The six-dimensional basis vectors $\mathbf{e}_i$ and $\mathbf{e}_i^*$ may be decomposed into parallel and orthogonal components:

$$\begin{aligned} \tilde{\mathbf{e}} &= \mathbf{e}^{\parallel} + \mathbf{e}^{\perp}; \\ \tilde{\mathbf{e}}^* &= \mathbf{e}^{*\parallel} + \mathbf{e}^{*\perp}; \end{aligned} \tag{7}$$

which can be expressed as

$$(\mathbf{e}^{\parallel})^T = A\begin{bmatrix} k & \mathbf{0} \\ \mathbf{0} & \boldsymbol{S}_l \end{bmatrix}\boldsymbol{E}^T, \tag{8a}$$

$$(\mathbf{e}^{\perp})^T = A\begin{bmatrix} \mathbf{0} & \mathbf{0} \\ \mathbf{0} & \boldsymbol{S}_r \end{bmatrix}\boldsymbol{E}^T, \tag{8b}$$

$$(\mathbf{e}^{*\parallel})^T = (1/A)\begin{bmatrix} 1/k & \mathbf{0} \\ \mathbf{0} & \boldsymbol{S}_l \end{bmatrix}\boldsymbol{E}^T \tag{9a}$$

and

$$(\mathbf{e}^{*\perp})^T = (1/A)\begin{bmatrix} \mathbf{0} & \mathbf{0} \\ \mathbf{0} & \boldsymbol{S}_r \end{bmatrix}\boldsymbol{E}^T, \tag{9b}$$

where $\mathbf{0}$ signifies that the rest of the row or column is composed of zeros. By inserting (6a) into (1) we

obtain

$$\boldsymbol{S}\boldsymbol{S}^T = \boldsymbol{I} \tag{10}$$

with $\boldsymbol{I}$ being a unit matrix. From (6) and (10) we obtain

$$\boldsymbol{E}^T = (1/A)\begin{bmatrix} 1/k & \mathbf{0} \\ \mathbf{0} & \boldsymbol{S}^T \end{bmatrix}\tilde{\mathbf{e}}^T \tag{11a}$$

and

$$\boldsymbol{E}^T = A\begin{bmatrix} k & \mathbf{0} \\ \mathbf{0} & \boldsymbol{S}^T \end{bmatrix}(\tilde{\mathbf{e}}^*)^T. \tag{11b}$$

Then, by inserting (11*a*) into (8*a*) we obtain an expression for the projection matrix $\boldsymbol{P}^{\parallel}$,

$$(\mathbf{e}^{\parallel})^T = \boldsymbol{P}^{\parallel}\tilde{\mathbf{e}}^T \tag{12a}$$

with

$$\boldsymbol{P}^{\parallel} = \begin{bmatrix} k & \mathbf{0} \\ \mathbf{0} & \boldsymbol{S}_1 \end{bmatrix}\begin{bmatrix} 1/k & \mathbf{0} \\ \mathbf{0} & \boldsymbol{S}_1{}^T \end{bmatrix}. \tag{12b}$$

Similarly, we have

$$(\mathbf{e}^{\perp})^T = \boldsymbol{P}^{\perp}\tilde{\mathbf{e}}^T \tag{13a}$$

with

$$\boldsymbol{P}^{\perp} = \begin{bmatrix} \mathbf{0} \\ \boldsymbol{S}_r \end{bmatrix}[\mathbf{0}\ \ \boldsymbol{S}_r^T] \tag{13b}$$

and

$$\boldsymbol{P}^{\parallel} + \boldsymbol{P}^{\perp} = \boldsymbol{I}. \tag{14}$$

2.2. *Index scheme for the decagonal phase*

For the decagonal phase we choose the 5×2 matrix $\boldsymbol{S}_1$ in (8*a*) as

$$\boldsymbol{S}_1 = (2/5)^{1/2}\begin{bmatrix} 1 & 0 \\ c_2 & s_2 \\ -c_1 & s_1 \\ -c_1 & -s_1 \\ c_2 & -s_2 \end{bmatrix}, \tag{15}$$

where

$$c_1 = \cos(2\pi/10) = \tau/2; \quad s_1 = \sin(2\pi/10) = (3-\tau)^{1/2}/2;$$

$$c_2 = \cos(2\pi/5) = 1/2\tau; \quad s_2 = \sin(2\pi/5) = (2+\tau)^{1/2}/2;$$

with $\tau = (1+5^{1/2})/2$ being the golden mean and

$$1 + 2c_1^2 + 2c_2^2 = 2s_1^2 + 2s_2^2 = 5/2;$$

$$s_1 s_2 + c_1 c_2 = s_2^2 - c_2^2 = c_1; \quad s_1 s_2 - c_1 c_2 = c_1^2 - s_1^2 = c_2.$$

Fig. 1(*a*) shows the relationship between $\mathbf{e}_i^{\parallel}$ and the unit vectors $\mathbf{E}_1$, $\mathbf{E}_2$, $\mathbf{E}_3$ in the parallel space as selected by (15). Inserting (15) into (12*b*) we get

$$\boldsymbol{P}^{\parallel} = (1/5)\begin{bmatrix} 5 & 0 & 0 & 0 & 0 & 0 \\ 0 & 2 & 1/\tau & -\tau & -\tau & 1/\tau \\ 0 & 1/\tau & 2 & 1/\tau & -\tau & -\tau \\ 0 & -\tau & 1/\tau & 2 & 1/\tau & -\tau \\ 0 & -\tau & -\tau & 1/\tau & 2 & 1/\tau \\ 0 & 1/\tau & -\tau & -\tau & 1/\tau & 2 \end{bmatrix} \tag{16}$$

and, from (14),

$$\boldsymbol{P}^{\perp} = (1/5)\begin{bmatrix} 0 & 0 & 0 & 0 & 0 & 0 \\ 0 & 3 & -1/\tau & \tau & \tau & -1/\tau \\ 0 & -1/\tau & 3 & -1/\tau & \tau & \tau \\ 0 & \tau & -1/\tau & 3 & -1/\tau & \tau \\ 0 & \tau & \tau & -1/\tau & 3 & -1/\tau \\ 0 & -1/\tau & \tau & \tau & -1/\tau & 3 \end{bmatrix}. \tag{17}$$

Inserting (17) into (13*a*), we obtain the mutual relationships between the $\mathbf{e}_j{}^{\perp}$,

$$|\mathbf{e}_j{}^{\perp}| = (3/5)^{1/2},$$

$$\cos(\mathbf{e}_j{}^{\perp}, \mathbf{e}_{j\pm1}{}^{\perp}) = -1/3\tau,$$

and

$$\cos(\mathbf{e}_j{}^{\perp}, \mathbf{e}_{j\pm2}{}^{\perp}) = \tau/3$$

for $j = 2, 3, 4, 5, 6$ and $\mathbf{e}_1{}^{\perp} = 0$. To fulfill these relationships we can select $\mathbf{e}_j{}^{\perp}$ as

$$(\mathbf{e}^{\perp})^T = A\begin{bmatrix} \mathbf{0} \\ \boldsymbol{S}_r \end{bmatrix}\begin{bmatrix} \mathbf{E}_4 \\ \mathbf{E}_5 \\ \mathbf{E}_6 \end{bmatrix} \tag{18a}$$

with

$$\boldsymbol{S}_r = (2/5)^{1/2}\begin{bmatrix} 1 & 0 & 1/2^{1/2} \\ -c_1 & s_1 & 1/2^{1/2} \\ c_2 & -s_2 & 1/2^{1/2} \\ c_2 & s_2 & 1/2^{1/2} \\ -c_1 & -s_1 & 1/2^{1/2} \end{bmatrix}, \tag{18b}$$

which are shown in Fig. 1(*b*).

A six-dimensional vector $\tilde{\mathbf{g}}$ may be expressed as

$$\tilde{\mathbf{g}} = \mathbf{n}^*\tilde{\mathbf{e}}^{*T} \tag{19a}$$

with

$$\mathbf{n}^* = [n_1{}^* n_2{}^* n_3{}^* n_4{}^* n_5{}^* n_6{}^*]$$

being the six-dimensional indices of $\mathbf{g}$ or

$$\tilde{\mathbf{g}} = \mathbf{g}^{\parallel} + \mathbf{g}^{\perp} \tag{19b}$$

with

$$\mathbf{g}^{\parallel} = (g_1{}^{\parallel}\, g_2{}^{\parallel}\, g_3{}^{\parallel})\begin{bmatrix} \mathbf{E}_1 \\ \mathbf{E}_2 \\ \mathbf{E}_3 \end{bmatrix} \tag{19c}$$

and

$$\mathbf{g}^{\perp} = (g_1{}^{\perp} g_2{}^{\perp} g_3{}^{\perp})\begin{bmatrix} \mathbf{E}_4 \\ \mathbf{E}_5 \\ \mathbf{E}_6 \end{bmatrix} \tag{19d}$$

being the components in physical and complementary spaces of the six-dimensional vector $\tilde{\mathbf{g}}$. Since the relationship between different components of a reciprocal vector is the same as between the corresponding basis vectors, from (11*a*) we have

$$\begin{bmatrix} g_1{}^{\parallel} \\ g_2{}^{\parallel} \\ g_3{}^{\parallel} \end{bmatrix} = (1/A)\begin{bmatrix} 1/k & \mathbf{0} \\ \mathbf{0} & \boldsymbol{S}_1{}^T \end{bmatrix}(\boldsymbol{n}^*)^T \tag{20}$$

and

$$\begin{bmatrix} g_1{}^{\perp} \\ g_2{}^{\perp} \\ g_3{}^{\perp} \end{bmatrix} = (1/A)\ [\mathbf{0}\ \boldsymbol{S}_r{}^T]\ (\mathbf{n}^*)^T. \tag{21}$$

Similarly, the components of a six-dimensional lattice vector

$$\tilde{\mathbf{R}} = \mathbf{n}\tilde{\mathbf{e}}^T = \mathbf{R}^{\parallel} + \mathbf{R}^{\perp} = [R_1{}^{\parallel}\ R_2{}^{\parallel}\ R_3{}^{\parallel}] \begin{bmatrix} \mathbf{E}_1 \\ \mathbf{E}_2 \\ \mathbf{E}_3 \end{bmatrix} + [R_1{}^{\perp} R_2{}^{\perp} R_3{}^{\perp}] \begin{bmatrix} \mathbf{E}_4 \\ \mathbf{E}_5 \\ \mathbf{E}_6 \end{bmatrix} \tag{22}$$

satisfy the relationships

$$\begin{bmatrix} R_1{}^{\parallel} \\ R_2{}^{\parallel} \\ R_3{}^{\parallel} \end{bmatrix} = A \begin{bmatrix} k & \mathbf{0} \\ \mathbf{0} & \boldsymbol{S}_1{}^T \end{bmatrix} \mathbf{n}^T \tag{23}$$

and

$$\begin{bmatrix} R_1{}^{\perp} \\ R_2{}^{\perp} \\ R_3{}^{\perp} \end{bmatrix} = A\ [\mathbf{0}\ \boldsymbol{S}_r{}^T]\ \mathbf{n}^T \tag{24}$$

with

$$\mathbf{n} = [n_1 n_2 n_3 n_4 n_5 n_6]$$

being the six-dimensional indices of $\tilde{\mathbf{R}}$.

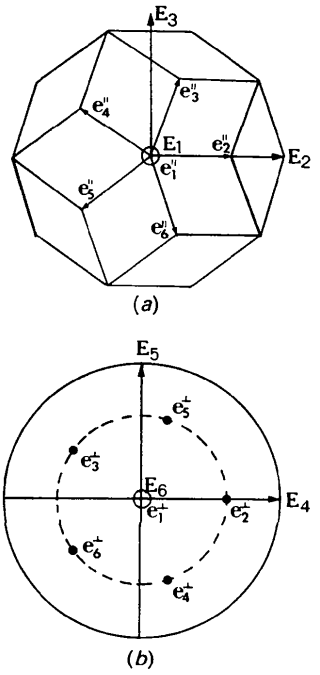

Fig. 1. (*a*) Diagram showing the physical-space components $\mathbf{e}_i^{\parallel}$ of the six-dimensional basis vectors $\tilde{\mathbf{e}}_i$. (*b*) Stereographic projection diagram showing the complementary space components $\mathbf{e}_i{}^{\perp}$ of the basis vectors $\tilde{\mathbf{e}}_i$. Each point shown is the endpoint of a vector $\mathbf{e}_i{}^{\perp}$

From (8*a*) and (15) the decagonal quasilattice parameters a and c are expressed as

$$a = (2/5)^{1/2}A, \quad c = kA, \tag{25a}$$

where a is the length of $\mathbf{e}_j^{\parallel}$ ($j = 2, 3, 4, 5, 6$) and c is the length of $\mathbf{e}_1{}^{\parallel}$. Similarly, the reciprocal decagonal quasilattice parameters a^* and c^* are expressed as

$$a^* = 2/(5a), \quad c^* = 1/c. \tag{25b}$$

In the case of crystals, the zone relation

$$\mathbf{R}\cdot\mathbf{g} = 0 \tag{26a}$$

is expressed as

$$[u\ v\ w] \begin{bmatrix} h \\ k \\ l \end{bmatrix} = 0, \tag{26b}$$

where $[u\ v\ w]$ are the indices of the zone $\mathbf{R}$ and $(h\ k\ l)$ are the indices of reciprocal vectors $\mathbf{g}$ belonging to the zone $\mathbf{R}$. However, from (20), (23) and (12*b*), the zone relation

$$\mathbf{R}^{\parallel}\cdot\mathbf{g}^{\parallel} = 0 \tag{26c}$$

in the case of decagonal quasicrystals should be expressed as

$$\mathbf{n}\boldsymbol{P}^{\parallel}\mathbf{n}^{*T} = 0. \tag{26d}$$

2.3. *Computer simulation*

In this work, we use a simplified formula to calculate the diffraction intensities,

$$I(\mathbf{g}) = f(\theta)\exp(-g^{\perp}), \tag{27}$$

where $f(\theta) = 0.7f_{Al}(\theta) + 0.15f_{Co}(\theta) + 0.15f_{Ni}(\theta)$ is the mean atomic scattering factor for $Al_{70}Co_{15}Ni_{15}$ decagonal phase and $g^{\perp}$ is the magnitude of $\mathbf{g}^{\perp}$. The variation of $f(\theta)$ with the Bragg angle θ is considered by the empirical expression

$$f(\theta) = \sum_{i=1}^{4} a_i \exp(-b_i \sin^2\theta/\lambda^2) + c, \tag{28}$$

where λ is the wavelength and a_i, b_i and c are constants, the values of which were fitted by Jiang & Li (1984).

According to the cut-and-projection method and the index system (§2.2), all six-dimensional reciprocal lattice vectors $\tilde{\mathbf{g}}(n_1^*, n_2^*, \ldots, n_6^*)$ with $0 \le n_1^* \le 3$, $-2 \le n_i^* \le 2$ ($i = 2, 3, \ldots, 6$) were projected onto the parallel space to obtain the three-dimensional reciprocal quasilattice vectors $\mathbf{g}^{\parallel}(n_1^*, n_2^*, \ldots, n_6^*)$. Only those $\mathbf{g}^{\parallel}$ with intensities larger than a given value I_{min} were output and the stereographic projections of the traces of the planes perpendicular to these $\mathbf{g}^{\parallel}$ were drawn. Fig. 2 shows such a stereographic projection diagram with only the 17 strongest traces. From Fig. 2, it can be seen that the zone axes *A*, *C*, *D*, *E*, *F*, *G*, *H*, *I*, *J'*, *J*, *K*, *M* and *N* labelled following the scheme evolved by Thangaraj *et al.*

(1987) and Daulton, Kelton & Gibbons (1991) are important at which some strong traces of planes intersect. With knowledge of the indices n_j* of these traces and a change of the indices n_j ($0 \le n_1 \le 4$ and $-8 \le n_j \le 8$ for other n_j) of possible zone axes, the indices of each zone axis were selected according to the zone relation (26*d*); see Table 1. Moreover, the real-space angles between the unique tenfold axis and other main zone axes have been calculated; see Table 2.

From the indices n_j* of the traces $\mathbf{g}^{\parallel}$ near a zone axis in Fig. 2 and calculation of their Bragg angles, a Kikuchi-line pattern of that zone axis can be obtained (Fig. 3). The indices, moduli and calculated intensities of the Kukuchi lines in Fig. 3 are listed in Table 3.

The simulation procedure of an SAED pattern of the zone axis $\mathbf{R}^{\parallel}$ is as follows. All the six-dimensional reciprocal lattice vectors $\tilde{\mathbf{g}}(n^*)$ with $-3 \le n_1^* \le 3$ and $-2 \le n_j^* \le 2$ for other n_j* are selected in turn and their corresponding three-dimensional vectors $\mathbf{g}^{\parallel}(n^*)$ are calculated according to (20). Only those reflections $\mathbf{g}^{\parallel}$ that satisfy the zone relation (26*d*) and have intensities larger than a given value $I_{\min}$ are output.

2.4. *Inflation and deflation*

According to Fig. 1(*a*) and equations (8*a*) and (15), if we select another basis vector set $\mathbf{e}^{\parallel\prime} = [\mathbf{e}_1^{\parallel\prime}\mathbf{e}_2^{\parallel\prime}\mathbf{e}_3^{\parallel\prime}\mathbf{e}_4^{\parallel\prime}\mathbf{e}_5^{\parallel\prime}\mathbf{e}_6^{\parallel\prime}]$ as

$$\mathbf{e}^{\parallel\prime} = \mathbf{e}^{\parallel}\boldsymbol{M} \tag{29}$$

Table 1. *Indices of the prominent 'zone axes' of* Al–Co–Ni *decagonal phase*

The pattern labels are those assigned in Fig. 2.

Pattern labels	Zone indices						Zone indices					
	n_1	n_2	n_3	n_4	n_5	n_6	n_1'	n_2'	n_3'	n_4'	n_5'	n_6'
A	1	0	0	0	0	0	1	0	0	0	0	0
C	1	−1	1	−2	0	2	1	−11	11	−7	0	7
D	1	2	−2	−1	0	1	1	7	−7	4	0	−4
E	1	−3	3	−6	0	6	1	−33	33	−21	0	21
F	1	6	−6	−3	0	3	1	21	−21	12	0	−12
G	0	1	−1	0	0	0	0	1	−1	0	0	0
H	0	0	0	0	0	1	0	0	0	0	0	1
I	1	7	−8	−8	7	7	1	37	7	7	37	−8
J	1	2	−3	−3	2	2	1	7	−3	−3	7	−8
M	1	3	−2	−2	3	−2	1	18	−7	−7	18	−22
N	2	−2	−2	−2	−2	3	2	−27	−12	−12	−27	−2

Table 2. *Real-space angles* (°) *between the unique tenfold axis and other prominent zone axes of* Al–Co–Ni *decagonal phase*

Pattern	*C*	*D*	*E*	*F*	*G*	*H*	*I*	*J*	*M*	*N*
Observed (±0.8°)	32.0	45.3	62.7	73.2	89.9	90.5	79.9	63.1	26.5	30.7
Calculated	31.82	45.11	61.75	71.63	90.00	90.00	80.10	62.36	36.11	30.54

with the inflation matrix

$$\boldsymbol{M} = \begin{bmatrix} 1 & 0 & 0 & 0 & 0 & 0 \\ 0 & 0 & 0 & -1 & -1 & 0 \\ 0 & 0 & 0 & 0 & -1 & -1 \\ 0 & -1 & 0 & 0 & 0 & -1 \\ 0 & -1 & -1 & 0 & 0 & 0 \\ 0 & 0 & -1 & -1 & 0 & 0 \end{bmatrix} \tag{30}$$

then we have $\mathbf{e}_1^{\parallel\prime} = \mathbf{e}_1^{\parallel}$ and $\mathbf{e}_j^{\parallel\prime} = \tau\mathbf{e}_j^{\parallel}$ ($j = 2, 3, \ldots, 6$).

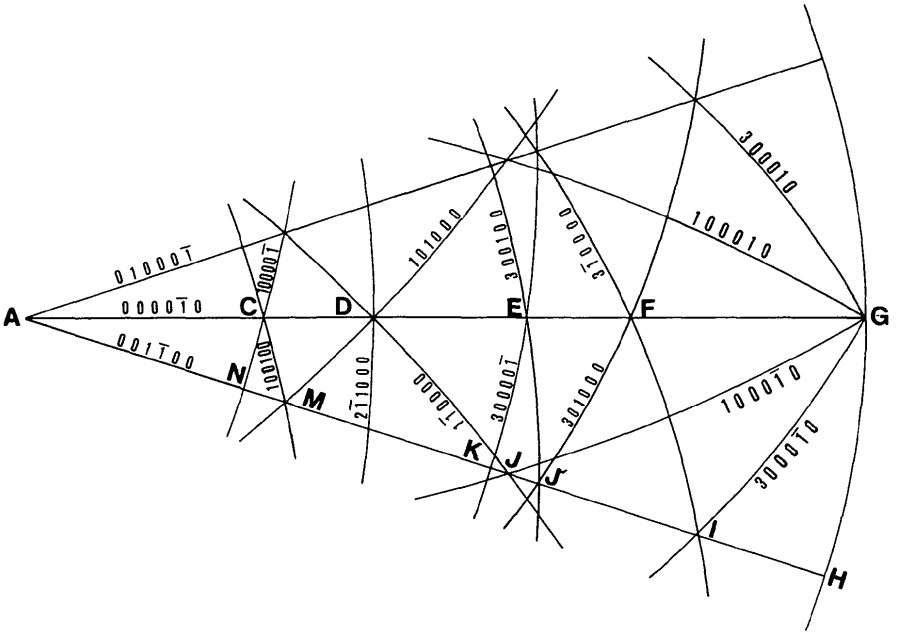

Fig. 2. Calculated stereographic projection diagram showing main traces of $Al_{70}Co_{15}Ni_{15}$ decagonal quasilattice planes and main zone axes *A*, *C*, *D*, *E*, *F*, *G*, *H*, *I*, *J'*, *J*, *K*, *M* and *N*.

The corresponding reciprocal basis $\mathbf{e}^{*\parallel\prime} = [\mathbf{e}_1^{*\parallel\prime}\mathbf{e}_2^{*\parallel\prime}\mathbf{e}_3^{*\parallel\prime}\mathbf{e}_4^{*\parallel\prime}\mathbf{e}_5^{*\parallel\prime}\mathbf{e}_6^{*\parallel\prime}]$ will be transformed as

$$(\mathbf{e}^{*\parallel\prime})^T = \boldsymbol{M}^*(\mathbf{e}^{*\parallel})^T \tag{31}$$

with

$$\boldsymbol{M}^* = (1/2)\begin{bmatrix} 2 & 0 & 0 & 0 & 0 & 0 \\ 0 & -1 & 1 & -1 & -1 & 1 \\ 0 & 1 & -1 & 1 & -1 & -1 \\ 0 & -1 & 1 & -1 & 1 & -1 \\ 0 & -1 & -1 & 1 & -1 & 1 \\ 0 & 1 & -1 & -1 & 1 & -1 \end{bmatrix} \tag{32}$$

and

$$\boldsymbol{M}\boldsymbol{M}^* = \boldsymbol{I}. \tag{33}$$

From (31) and (32) we have

$$\mathbf{e}_1^{*\parallel\prime} = \mathbf{e}_1^{*\parallel} \quad \text{and} \quad \mathbf{e}_j^{*\parallel\prime} = (1/\tau)\mathbf{e}_j^{*\parallel} \quad (j = 2, 3, \ldots, 6).$$

Therefore, the indices of $\mathbf{g}^{\parallel}$ and $\mathbf{R}^{\parallel}$ will be correspondingly transformed as

$$\mathbf{n}^{*\prime} = \mathbf{n}^*\boldsymbol{M} \tag{34}$$

and

$$(\mathbf{n}')^T = \boldsymbol{M}^*\mathbf{n}^T. \tag{35}$$

Such an inflation property means that the indexing of the reflections of the decagonal quasicrystal is not unique. The indices of all reflections and zone axes may be inflated and deflated according to the matrices $\boldsymbol{M}$ and $\boldsymbol{M}^*$, respectively, and the magnitudes of the basis vectors $\mathbf{a}^*$ and $\mathbf{a}$ are correspondingly deflated and inflated by the factors of $1/\tau$ and τ, respectively.

3. Experimental

3.1. *Experimental method*

The $Al_{70}Co_{15}Ni_{15}$ alloy was prepared by melting the pure metals using a high-frequency induction furnace under an Ar atmosphere. After it had cooled to room temperature, the ingot was annealed in a vacuum furnace at 1100 K for 48 h and then cut into slices from which thin-foil specimens for transmission electron microscopy (TEM) were prepared by mechanical thinning and subsequent ion-milling. A Phillips EM-420 transmission electron microscope was used at an accelerating voltage of 100 kV to obtain the diffraction contrast images, SAED patterns and Kikuchi patterns. The latter were obtained

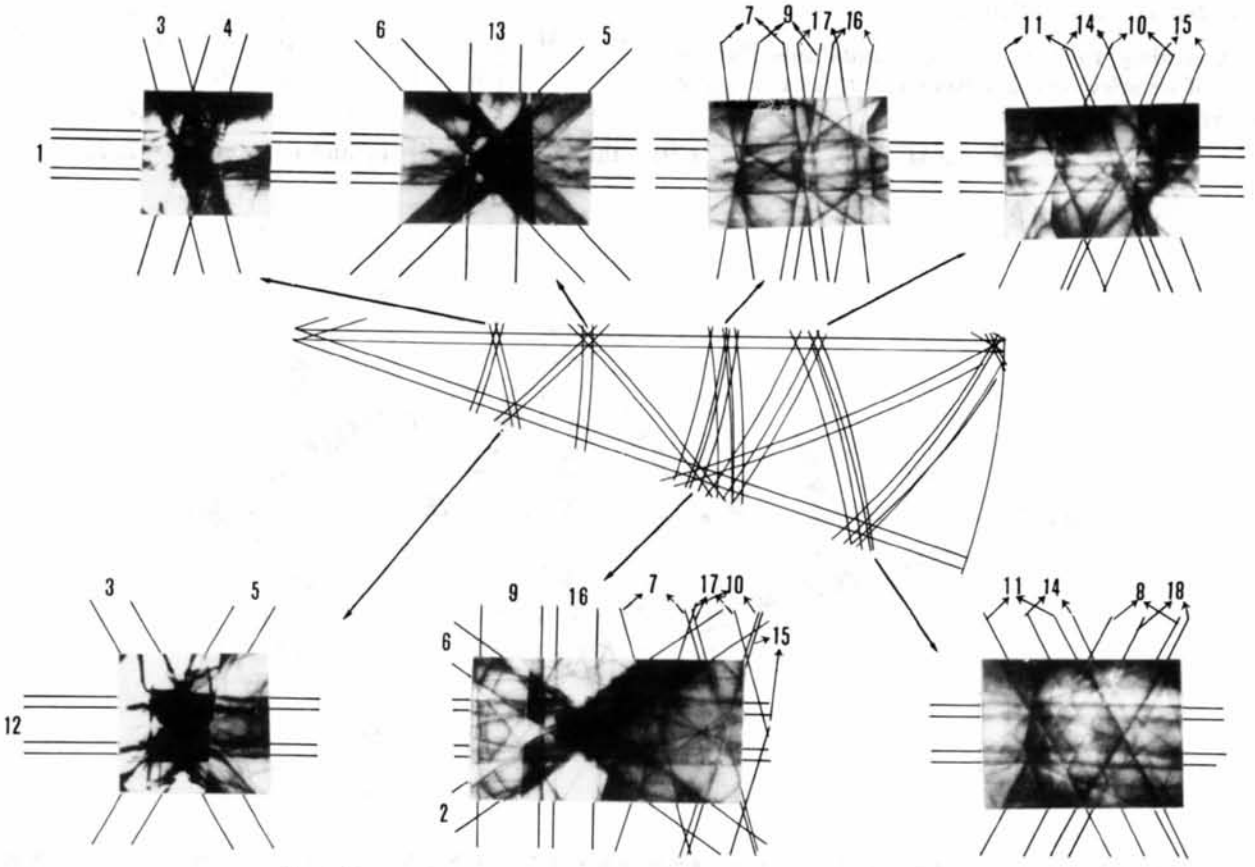

Fig. 3. Comparisons of experimental and simulated Kikuchi-line patterns.

Table 3. *The indices and the moduli of the Kikuchi lines in Fig.* 3

No.	n_1^*	n_2^*	n_3^*	n_4^*	n_5^*	n_6^*	$n_1^{*\prime}$	$n_2^{*\prime}$	$n_3^{*\prime}$	$n_4^{*\prime}$	$n_5^{*\prime}$	$n_6^{*\prime}$	$g^{\parallel}$	I/I_1
1	0	0	0	0	−1	0	0	2	2	−1	−3	−1	0.41	1.00
	0	0	0	0	1	0	0	−2	−2	1	3	1		
2	1	0	0	0	−1	0	1	2	2	−1	−3	−1	0.48	0.84
	−1	0	0	0	1	0	−1	−2	−2	1	3	1		
3	1	0	0	1	0	0	1	−2	1	3	1	−2	0.48	0.84
	−1	0	0	−1	0	0	−1	2	−1	−3	−1	2		
4	1	0	0	0	0	−1	1	−1	2	2	−1	−3	0.48	0.84
	−1	0	0	0	0	1	−1	1	−2	−2	1	3		
5	1	0	1	0	0	0	1	1	3	1	−2	−2	0.48	0.84
	−1	0	−1	0	0	0	−1	−1	−3	−1	2	2		
6	1	−1	0	0	0	0	1	−3	−1	2	2	−1	0.48	0.84
	−1	1	0	0	0	0	−1	3	1	−2	−2	1		
7	3	0	0	1	0	0	3	−2	1	3	1	−2	0.48	0.41
	−3	0	0	−1	0	0	−3	2	−1	−3	−1	2		
8	3	0	0	0	−1	0	3	2	2	−1	−3	−1	0.84	0.41
	−3	0	0	0	1	0	−3	−2	−2	1	3	1		
9	3	0	0	0	0	−1	3	−1	2	2	−1	−3	0.84	0.41
	−3	0	0	0	0	1	−3	1	−2	−2	1	3		
10	3	0	1	0	0	0	3	1	3	1	−2	−2	0.84	0.41
	−3	0	−1	0	0	0	−3	−1	−3	−1	2	2		
11	3	−1	0	0	0	0	3	−3	−1	2	2	−1	0.84	0.41
	−3	1	0	0	0	0	−3	3	1	−2	−2	1		
12	0	0	1	−1	0	0	0	3	2	−2	−3	0	0.49	0.36
	0	0	−1	1	0	0	0	−3	−2	2	3	0		
13	2	−1	1	0	0	0	2	−2	2	3	0	−3	0.69	0.23
	−2	1	−1	0	0	0	−2	2	−2	−3	0	3		
14	2	0	−1	0	0	−1	2	−2	−1	1	1	−1	0.55	0.21
	−2	0	1	0	0	1	−2	2	1	−1	−1	1		
15	2	1	0	1	0	0	2	1	2	1	−1	−1	0.55	0.21
	−2	−1	0	−1	0	0	−2	−1	−2	−1	1	1		
16	2	−1	0	0	−1	0	2	−1	1	1	−1	−2	0.55	0.21
	−2	1	0	0	1	0	−2	1	−1	−1	1	2		
17	2	0	1	0	1	0	2	−1	1	2	1	−1	0.55	0.21
	−2	0	−1	0	−1	0	−2	1	−1	−2	−1	1		
18	2	0	0	1	0	1	2	1	1	−1	−2	−1	0.55	0.21
	−2	0	0	−1	0	−1	−2	−1	−1	1	2	1		

in this work mainly by elastic scattering under the large-angle convergent-beam electron diffraction (LACBED) mode (Williams, 1984).

3.2. *SAED patterns*

$Al_{70}Co_{15}Ni_{15}$ thin foils consist of grains of the decagonal phase. Fig. 4(*a*) shows a near-twofold-axis bright-field image, where thin needles with zebra-contrast, parallel to the projection of the tenfold axis, can be seen. Fig. 4(*b*) shows the SAED pattern along the tenfold axis obtained from the Al–Co–Ni decagonal phase.

SAED patterns of main zone axes were photographed and the readings of the double-tilting goniometer at each zone axis were taken. From these readings the experimental angles between the unique tenfold axis and other main zone axes were obtained; they show good agreement with the calculated values (see Table 2).

The main characteristics of the *C*, *D*, *M* and *N* zone-axis SAED patterns for Al–Co–Ni decagonal phase are the same as for Al–Mn (FitzGerald, Withers, Stewart & Calka, 1988; Choy *et al.*, 1988) but the *J* and *G* patterns (see Figs. 5*a*, 5*b*) are different from the corresponding *J* and *G* patterns for Al–Mn. In the Al–Mn decagonal phase, the *J* zone-axis SAED pattern is a degenerate fivefold pattern but Fig. 5(*a*) does not show any fivefold symmetry. In the *G* pattern shown in Fig. 5(*b*) there are six strong spots labelled as 8 and 10, forming a hexagon corresponding to a lattice-plane spacing of 2 Å. This characteristic is the same for all decagonal phases with periodicities an integral multiple of 4 Å, as shown by He *et al.* (1988). The reciprocal vector corresponding to spot 10 is divided into two parts by the horizontal spot row consisting of strong reflections (see Fig. 5*b*) for the Al–Co–Ni decagonal phase, which corresponds to the periodicity of 4 Å, while it is divided into four, six and eight parts for other decagonal phases with periodicities 8, 12 and 16 Å respectively (He *et al.*, 1988). The presence of the horizontal weak diffraction streaks suggests an 8 Å periodicity parallel to the tenfold axis. These streaks may originate from thin needle-like order domains along the tenfold axis. Since these streaks are very weak, as a first-order approximation we neglect their contribution to simulated Kikuchi-line and SAED patterns.

Firstly, we assign indices of (0 0 0 0 −1 0) to the arrowed reflection 7 in Fig. 5(*b*) and indices of (2 0 0 0 0 0) to reflection 10. The ratio of the magnitudes of these two reciprocal vectors is measured from Fig. 5(*b*) to be 0.85 (5), from which the co-

efficient $1/k$ is calculated to be 0.37 by use of (20). Under this indexing the quasilattice parameters for the $Al_{70}Co_{15}Ni_{15}$ decagonal phase are determined to be $a = 0.98$ and $c = 4.0$ Å.

SAED patterns of all zone axes labelled in Fig. 1 were simulated; they are in good agreement with experimental patterns except that the diffuse streaks similar to those shown in Fig. 5 were not simulated. Fig. 5 shows a comparison of the experimental (upper parts) and simulated (lower parts) SAED patterns of J (Fig. 5*a*) and G (Fig. 5*b*) zone axes. The indices and moduli of reflections labelled in Fig. 5 are listed in Table 4. By comparison of the simulated and experimental SAED patterns, the diffraction spots in the experimental SAED patterns can be indexed.

3.3. *Kikuchi-line patterns*

Fig. 3 shows composite experimental Kikuchi patterns compared with the simulated patterns. The indices of the Kikuchi lines labelled in Fig. 3 and the moduli of the corresponding reciprocal vectors are listed in Table 3. From a comparison of the experimental and simulated Kikuchi-line patterns, it is evident that their characteristics agree rather well with each other except that some experimental Kikuchi lines are bent owing to local bending of the foil specimen.

3.4. *Inflation of the basis sets and indices*

The quasilattice parameter $a = 0.98$ Å as determined in §3.2 does not possess any physical meaning because it is smaller than conventional atomic distances. By inflation of the basis set by the inflation matrix $\boldsymbol{M}^4$, the quasilattice parameters are changed to $c' = c = 4$ Å and $a' = \tau^4 a = 6.6$ Å. This value of a' is in accordance with the atomic decoration of the decagonal Penrose lattice as proposed by Li & Kuo (1992). According to (34) and (35), the indices $\mathbf{n}^*$ and $\mathbf{n}$ of the reciprocal vectors and the zone axes are changed into $\mathbf{n}^{*\prime}$ and $\mathbf{n}'$, respectively. They are listed in Tables 1, 3 and 4. If the basis set is inflated by the matrix $\boldsymbol{M}^2$ then the quasilattice parameters will be changed to $c'' = c$ and $a'' = \tau^2 a = 2.5$ Å. This value of a'' corresponds exactly to the atomic distance of the decagonal quasicrystals. In this case the atoms are situated at the Penrose lattice points with some vacant positions.

4. Discussion

From the similarity of some SAED patterns of the decagonal Al–Mn and the isosahedral Al–Mn quasicrystals, Fung *et al.* (1986) described the decagonal phase by the relationship between these two types of quasicrystals. FitzGerald *et al.* (1988) abandoned this description. Our investigation of the

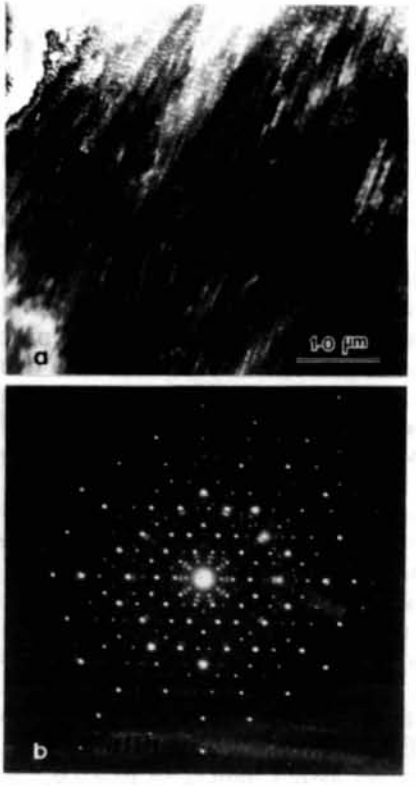

Fig. 4. (*a*) A near-twofold-axis bright-field image of the $Al_{70}Co_{15}Ni_{15}$ decagonal phase. The striations with zebra constrast are parallel to the local tenfold axis projection. (*b*) The SAED pattern of the Al–Co–Ni decagonal phase along the tenfold axis.

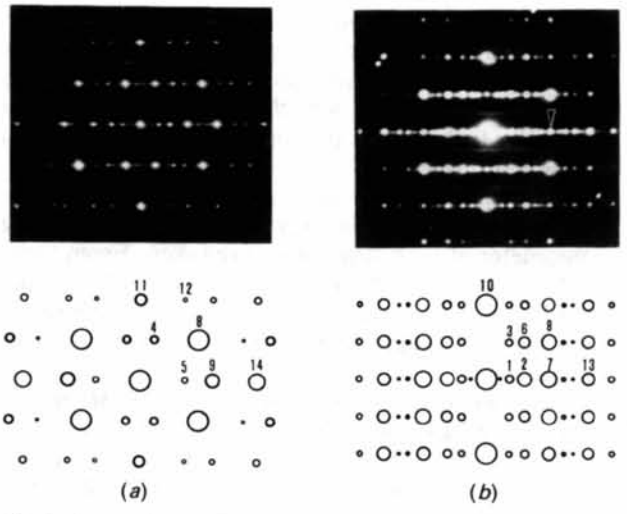

Fig. 5. Comparisons of experimental (upper parts) and simulated (lower parts) SAED patterns corresponding to (*a*) J and (*b*) G zone axes.

Table 4. *The indices and moduli for the labelled reflections in Fig. 5*

No.	n_1^*	n_2^*	n_3^*	n_4^*	n_5^*	n_6^*	$n_1^{*\prime}$	$n_2^{*\prime}$	$n_3^{*\prime}$	$n_4^{*\prime}$	$n_5^{*\prime}$	$n_6^{*\prime}$	$g^{\parallel}$
1	0	0	0	1	−1	1	0	2	2	1	0	1	0.16
2	0	0	0	−1	0	−1	0	−1	−1	1	2	1	0.26
3	1	0	0	1	−1	1	1	2	2	1	0	1	0.29
4	1	−1	1	−1	0	0	1	−1	0	−1	−2	−2	0.29
5	0	1	−1	1	−1	0	0	2	1	−1	−2	0	0.30
6	1	0	0	−1	0	−1	1	−1	−1	1	2	1	0.35
7	0	0	0	0	−1	0	0	2	2	−1	−3	−1	0.41
8	1	0	0	0	−1	0	1	2	2	−1	−3	−1	0.48
9	0	0	1	−1	0	0	0	3	2	−2	−3	0	0.49
10	2	0	0	0	0	0	2	0	0	0	0	0	0.49
11	2	−1	0	0	−1	0	2	−1	1	1	−1	−2	0.55
12	2	1	1	0	1	−1	2	1	4	2	−2	−3	0.60
13	0	1	1	0	0	0	0	4	4	−1	−4	1	0.64
14	0	1	0	0	−1	0	0	5	3	−3	−5	0	0.79

$Al_{70}Co_{15}Ni_{15}$ decagonal phase with a periodicity of 4 Å supports further the suggestion made by FitzGerald *et al.* (1988). The strongest argument for this is the *J* pattern (Fig. 5*a*), which does not show any fivefold symmetry. The degenerate fivefold symmetry of the *J* pattern in the Al–Mn decagonal phase is only a chance event, caused when the periodicity along the tenfold axis is 12 Å.

FitzGerald *et al.* (1988) stated that "most of the reciprocal-lattice points contributing to a 'zone-axis' pattern do not lie exactly normal to the 'zone-axis' direction" and cited the degenerate fivefold *J* pattern as an example. Our work shows that there are indeed rigorous zone relations $\mathbf{R}^{\parallel}\cdot\mathbf{g}^{\parallel} = 0$ for the decagonal phase. The most important stage is to select correctly the indices $\mathbf{n}$ of a zone axis according to the expression $\mathbf{n}\boldsymbol{P}^{\parallel}\mathbf{n}^* = 0$ from several known indices $\mathbf{n}^*$ of the reciprocal lattice vectors. Moreover, the so-called degenerate fivefold *J* pattern of the Al–Mn decagonal phase comes from two zones with very small interangle.

By use of the inflation and deflation properties one can choose an appropriate quasilattice parameter *a* as the edge length of the Penrose tiling. The value $a = 0.98$ Å does not possess any physical meaning because it is too small for atomic decoration. The three-times inflated parameter $a' = \tau^3 a = 4.0$ Å is exactly the value used by Zhang & Kuo (1990) and the four-times inflated parameter $a' = \tau^4 a = 6.6$ Å is very suitable for the structure model proposed by Li & Kuo (1992).

The general principle of the method described in this paper can be applied to other decagonal phases with different periodicities along the tenfold axis if the parameter *k* in (1) is changed. It can also be applied to other two-dimensional quasicrystals such as octagonal or dodecagonal phases. After some minor variations, this method can also be applied to the icosahedral and cubic quasicrystals.

References

BENDERSKY, L. (1985). *Phys. Rev. Lett.* **55**, 1461–1463.

CHATTOPADHYAY, K., LELE, S., RANGANATHAN, S., SUBBANNA, G. N. & THANGARAJ, N. (1985). *Curr. Sci.* **54**, 895–903.

CHOY, T. C., FITZGERALD, J. D. & KALLONIATIS, A. C. (1988). *Philos. Mag.* **B58**, 35–46.

DAULTON, T. L., KELTON, K. F. & GIBBONS, P. C. (1991). *Philos. Mag.* **B63**, 687–714.

DONG, C., LI, G. B. & KUO, K. H. (1987). *J. Phys. F*, **17**, L189–192.

ELSER, V. (1985). *Phys. Rev. B*, **32**, 4892–4898.

FITZGERALD, J. D., WITHERS, R. L., STEWART, A. M. & CALKA, A. (1988). *Philos. Mag.* **B58**, 15–34.

FUNG, K. K., YANG, C. Y., ZHOU, Y. Q., ZHAO, J. G., ZHAN, W. S. & SHEN, B. G. (1986). *Phys. Rev. Lett.* **56**, 2060–2063.

HE, L. X., WU, Y. K. & KUO, K. H. (1988). *J. Mater. Sci. Lett.* **7**, 1284–1286.

HO, T. L. (1986). *Phys. Rev. Lett.* **56**, 468–471.

IDZIAK, S., HEINEY, P. A. & BANCEL, P. A. (1987). *Mater. Sci. Forum*, **22–24**, 353–367.

JARIC, M. V. (1986). *Phys. Rev. B*, **34**, 4685–4698.

JIANG, J. S. & LI, F. H. (1984). *Acta Phys. Sin.* **33**, 845–850. (In Chinese.)

KATZ, A. & DUNEAU, M. (1986). *J. Phys. (Paris)*, **47**, 181–196.

KOOPMANS, B., SCHURER, P. J., VAN DER WOUDE, F. & BRONSVELD, P. (1987). *Phys. Rev. B*, **35**, 3005–3008.

LI, X. Z. & KUO, K. H. (1988). *Philos. Mag. Lett.* **58**, 167–171.

LI, X. Z & KUO, K. H. (1992). *Philos. Mag.* In the press.

MANDAL, R. K. & LELE, S. (1989). *Phys. Rev. Lett.* **62**, 2695–2698.

MANDAL, R. K. & LELE, S. (1991). *Philos. Mag.* **B63**, 513–527.

SURYANARAYANA, C. & MENON, J. (1987). *Scr. Metall.* **21**, 459–464.

THANGARAJ, N., SUBBANNA, G. N., RANGANATHAN, S. & CHATTOPADHYAY, K. (1987). *J. Microsc. (Oxford)*, **146**, 287–302.

TSAI, A. P., INOUE, A. & MASUMOTO, T. (1989). *Mater. Trans.* **30**, 150–154.

WILLIAMS, D. B. (1984). *Practical Analytical Electron Microscopy in Materials Science*, p. 126. Mahwah, New Jersey: Philips Electronic Instruments Inc.

ZHANG, H. & KUO, K. H. (1990). *Phys. Rev. B*, **42**, 8907–8913.